



OPEN ACCESS

EDITED BY

Eduardo Abreu,
University of Missouri–Kansas City,
United States

REVIEWED BY

Zheng Wang,
Wuhan University, China
Baolong Li,
Jilin University, China

*CORRESPONDENCE

Jun Liu
✉ liujun510999812@163.com

RECEIVED 05 June 2024

ACCEPTED 17 March 2025

PUBLISHED 03 April 2025

CITATION

Wei W, Zhang Z, Li B, Fu Z and Liu J (2025)
Deciphering the role of lncRNA-mediated
ceRNA network in disuse osteoporosis:
insights from bone marrow mesenchymal
stem cells under simulated microgravity.
Front. Med. 12:1444165.
doi: 10.3389/fmed.2025.1444165

COPYRIGHT

© 2025 Wei, Zhang, Li, Fu and Liu. This is an
open-access article distributed under the
terms of the [Creative Commons Attribution
License \(CC BY\)](https://creativecommons.org/licenses/by/4.0/). The use, distribution or
reproduction in other forums is permitted,
provided the original author(s) and the
copyright owner(s) are credited and that the
original publication in this journal is cited, in
accordance with accepted academic
practice. No use, distribution or reproduction
is permitted which does not comply with
these terms.

Deciphering the role of lncRNA-mediated ceRNA network in disuse osteoporosis: insights from bone marrow mesenchymal stem cells under simulated microgravity

Wuzeng Wei^{1,2}, Zhongli Zhang^{1,2}, Bing Li^{1,2}, Zhe Fu^{1,2} and Jun Liu^{1,2*}

¹Department of Orthopaedics, Tianjin Hospital, Tianjin University, Tianjin, China, ²Clinical College of Orthopedics, Tianjin Medical University, Tianjin, China

Background: Disuse osteoporosis (DOP) poses a significant health risk during extended space missions. Although the importance of long non-coding RNA (lncRNA) in bone marrow mesenchymal stem cells (BMSCs) and orthopedic diseases is recognized, the precise mechanism by which lncRNAs contribute to DOP remains elusive. This research aims to elucidate the potential regulatory role of lncRNAs in DOP.

Methods: Sequencing data were obtained from Gene Expression Omnibus (GEO) datasets, including coding and non-coding RNAs. Positive co-expression pairs of lncRNA-mRNA were identified using weighted gene co-expression network analysis, while miRNA-mRNA expression pairs were derived from the prediction database. A mRNA-miRNA-lncRNA network was established according to the shared mRNA. Functional enrichment analysis was conducted for the shared mRNAs using genome ontology and KEGG pathways. Hub genes were identified through protein-protein interaction analysis, and connectivity map analysis was employed to identify potential therapeutic agents for DOP.

Results: Integration of 74 lncRNAs, 19 miRNAs, and 200 mRNAs yielded a comprehensive mRNA-miRNA-lncRNA network. Enrichment analysis highlighted endoplasmic reticulum stress and extracellular matrix (ECM) pathways as significant in the ceRNA network. PPI analysis revealed three hub genes (COL4A1, LAMC1, and LAMA4) and identified five lncRNA-miRNA-hub gene regulatory axes. Furthermore, three potential therapeutic compounds (SB-216763, oxymetholone, and flubendazole) for DOP were identified.

Conclusion: This study sheds light on the involvement of lncRNAs in the pathogenesis and treatment of DOP through the construction of a ceRNA network, linking protein-coding mRNA functions with non-coding RNAs.

KEYWORDS

disuse osteoporosis, lncRNA, WGCNA, competing endogenous RNAs, BMSCs, CMAP

1 Introduction

While space exploration captivates our imagination, it also presents a spectrum of short- and long-term health challenges for astronauts (1). One of the most critical concerns is disuse osteoporosis (DOP), a condition characterized by accelerated bone loss due to mechanical unloading in microgravity environments (2, 3). Astronauts can experience a bone mass reduction of up to 2% per month during spaceflight, equivalent to more than a year's worth of bone loss in postmenopausal women (4). Disuse osteoporosis (DOP), arising from skeletal mechanical unloading, underscores the importance of investigating bone health under microgravity conditions (5).

Bone homeostasis depends on the balance between bone resorption by osteoclasts and bone formation by osteoblasts, processes critically regulated by bone marrow mesenchymal stem cells (BMSCs) (6, 7), which can differentiate into various cell types, including osteocytes, osteoblasts, chondrocytes, adipocytes, and smooth muscle cells (8). Strict regulation of BMSC differentiation is pivotal for maintaining bone homeostasis, as even minor disruptions can lead to orthopedic diseases such as osteoporosis (9). Although previous studies have explored the involvement of protein-coding genes in BMSC differentiation, increasing evidence suggests that non-coding RNAs, including long non-coding RNAs (lncRNAs) and microRNAs (miRNAs), also play pivotal regulatory roles in this process.

Long non-coding RNA (lncRNA), a subgroup of non-coding RNAs exceeding 200 nucleotides in length, have emerged as key players in diverse cellular processes such as cell differentiation, apoptosis, gene regulation, and cancer progression (10). Recent research has implicated lncRNAs in the regulation of osteogenic differentiation in BMSCs, with aberrant expression potentially disrupting bone homeostasis (11). For instance, decreased expression of lncRNA-H19, induced by mechanical unloading, has been linked to DOP development through Wnt signaling inhibition via increased Dkk4 expression. MiRNAs are known to modulate bone metabolism under mechanical stress and are associated with disuse-induced osteopenia or osteoporosis (12). lncRNAs regulate gene expression through various mechanisms, including acting as ceRNAs that sequester miRNAs from their target mRNAs. This competitive mechanism forms lncRNA-miRNA-mRNA networks, which are involved in many physiological and pathological processes (13). While their importance is recognized, few studies have explored the roles of competing endogenous RNAs (ceRNA) networks in DOP, particularly under microgravity conditions. Understanding these networks could provide valuable insights into the molecular mechanisms of DOP and reveal novel therapeutic targets.

This study addresses a critical gap in the understanding of DOP by focusing on the underexplored role of non-coding RNAs (ncRNAs), particularly lncRNAs, in regulating bone homeostasis under microgravity conditions. While previous research has primarily focused on protein-coding genes, our work highlights the complex interplay within lncRNA-miRNA-mRNA networks and their involvement in key processes, such as endoplasmic reticulum (ER) stress and extracellular

matrix (ECM) remodeling. By constructing a comprehensive competitive endogenous RNA (ceRNA) network through multi-omics integration, this study not only advances the molecular understanding of DOP but also identifies novel therapeutic targets.

Furthermore, the use of weighted gene co-expression network analysis (WGCNA) allowed us to systematically identify key regulatory axes, while Connectivity Map (CMap) analysis revealed bioactive compounds with strong translational potential, including SB-216763, oxymetholone, and flubendazole. These findings provide a foundation for developing targeted therapeutic strategies for DOP, bridging the gap between bioinformatics insights and practical applications. By filling these research gaps, our study paves the way for more effective prevention and treatment of DOP, offering significant benefits for astronauts and patients with osteoporosis caused by prolonged bed rest.

2 Materials and methods

A summary of the analysis procedure employed in this study is presented in Figure 1, while fundamental details regarding the two microarray datasets are outlined in Table 1.

2.1 GEO datasets

The relevant RNA sequencing data and microarray data were extracted from the Gene Expression Omnibus (GEO) database¹. RNA expression profiles were derived from GSE100930 (Microarray on mRNA and lncRNA, comprising seven flight samples and six ground samples) and GSE100932 (miRNA-seq, including six flight samples, and three ground samples). These datasets were generated using the platforms GPL6244 [HuGene-1_0-st] and GPL11154 [Illumina HiSeq 2000], as initially described by Bradamante and co-workers.

2.2 Data preprocessing

The Bioconductor software package 3.8² and the R v.3.5.2³ were utilized to preprocess the gene expression datasets. Specifically, the R software was employed via the Agilent platform to conduct preprocessing and normalization of the Series Matrix Files (.TXT files). Principal component analysis (PCA), a mathematical algorithm commonly integrated into genome-wide expression studies, was employed. PCA condenses data while preserving the bulk of its variability, facilitating visual assessment of sample similarities and differences and enabling grouping determination (14). In this study, PCA was conducted using the PRCOMP function in R software based on singular value decomposition (SVD) of the data matrix.

1 <http://www.ncbi.nlm.nih.gov/geo/>

2 <https://www.bioconductor.org/>

3 <https://www.r-project.org>

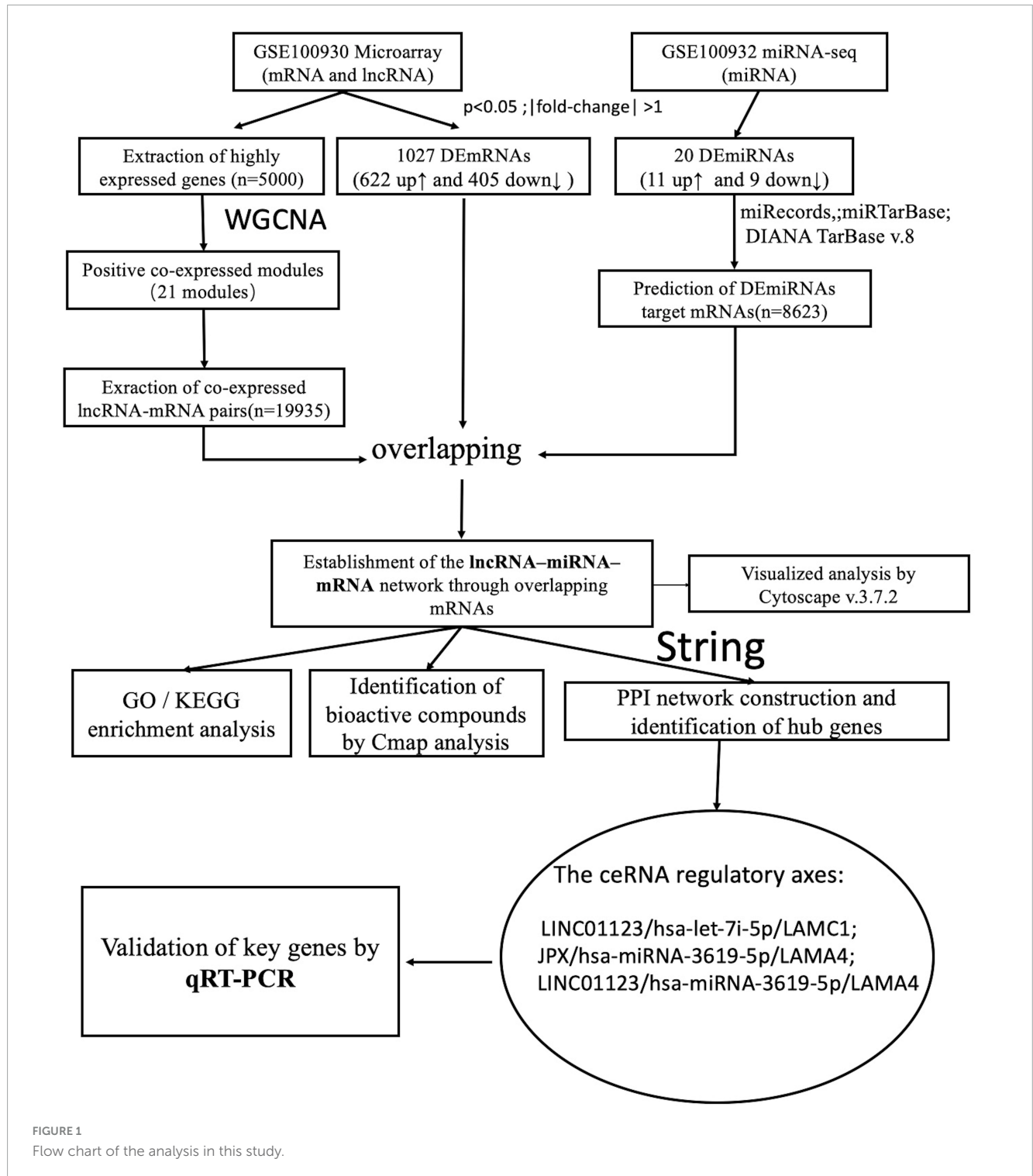


TABLE 1 Basic information on the two datasets from Gene Expression Omnibus (GEO).

GEO datasets	Year	Country	Platform	Sample	N	Detected RNA type
GSE100930	2019	Italy	GPL6244	Flight Ground	7 6	mRNA and lncRNA
GSE100932	2019	Italy	GPL11154	Flight Ground	6 3	miRNA

2.3 Identification of DEmRNAs and DEmiRNAs

The limma package in R was employed to perform differential expression analysis of microarray data between Flight and Ground conditions, focusing on mRNA expression changes. Meanwhile, for miRNAs, the edgeR package in R was utilized with RNA sequencing data. A significance threshold of $p < 0.05$ and a \log_2 (fold-change) > 1 were utilized as cut-off thresholds.

2.4 Prediction of target mRNAs for DEmiRNAs

The multiMiR package in R, comprising 14 databases, was used to predict miRNA-mRNA interactions. The predictions mainly employed data from three databases: miRecords, miRTarBase⁴ and DIANA TarBase v.8.

2.5 Construction of co-expressed gene module for lncRNA-mRNA pairs

Weighted gene co-expression network analysis is a state-of-the-art technique for deciphering co-expression patterns among genes (15). Firstly, from the GSE100930 dataset, 5,000 genes exhibiting the highest average expression were identified. Subsequently, the soft-thresholding power was measured, guided by the criterion of approximate scale-free topology fitting indices R^2 , whereby the β value was selected once R^2 achieved 0.85. Employing the appropriate soft threshold ($\beta = 12$), the weighted network underwent transformation into a topological overlap matrix (TOM), utilized thereafter to compute a gene's network connectivity. Following this, average linkage hierarchical clustering was performed using the TOM-based dissimilarity measure, enabling the classification of genes with analogous expression profiles into distinct gene modules. Ultimately, to acquire positive lncRNA-mRNA co-expression pairs from the gene modules, the TOMType parameter in the WGCNA package was designated as "signed." The detailed code is in the [Supplementary Data Sheets 1, 2](#).

2.6 Establishment of the mRNA-miRNA-lncRNA network

The positive lncRNA-mRNA co-expression pairs and miRNA-mRNA expression pairs were integrated based on shared mRNAs, with those containing DEmRNAs being filtered out. All mRNA-miRNA-lncRNA regulatory axes constituted the ceRNA network, which was visualized using Cytoscape v.3.7.2.

2.7 Enrichment analysis

Functional annotation of the DEmRNAs within the ceRNA network was conducted using the clusterProfiler package in R. GO terms were employed for functional enrichment analysis, while KEGG pathways were utilized for pathway enrichment analysis. A threshold of $p < 0.05$ was utilized as the cutoff for reporting significant GO terms and KEGG pathways.

2.8 Establishment of PPI network and identification of hub genes

The genes identified through the aforementioned analyses were cross-referenced with the STRING database⁵ to construct a PPI network. Interactions were restricted to Homo sapiens to ensure the relevance of the results to human biology. A confidence score threshold of ≥ 0.4 (medium confidence) was set to ensure that only interactions with appropriate evidence were included in the analysis. Additionally, the constructed PPI network was imported into Cytoscape software (version 3.7.2) for visualization and analysis. Finally, the CytoHubba plugin in Cytoscape software was utilized to identify the top 10 hub genes using the Maximal Clique Centrality (MCC) algorithm.

2.9 CMap query

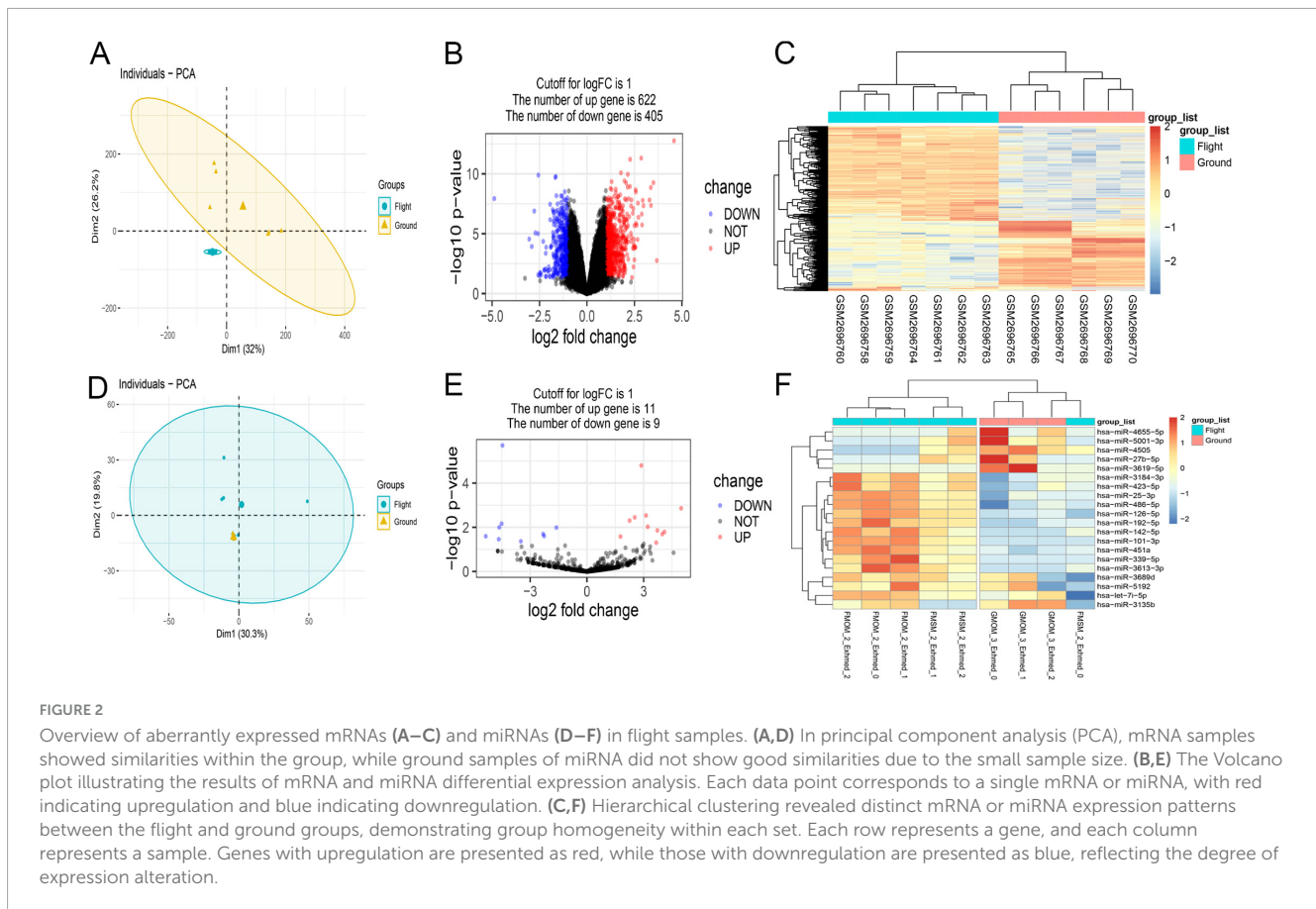
The CMap dataset of cellular signatures captures the transcriptional responses of human cells to both genetic and chemical perturbations. This comprehensive dataset encompasses profiles of 27,927 perturbagens, resulting in a total of 476,251 expression signatures (16). Subsequently, the upregulated and downregulated genes were compiled into respective upregulated and downregulated signatures, accessible via <https://clue.io>. Using pattern-matching algorithms, connectivity scores were computed to discern functional associations among drugs, genes, and diseases based on shared gene expression changes. These scores represent the degree of similarity with the expression profile, enabling the identification of bioactive compounds with the lowest connectivity scores, which are deemed potential therapeutic drugs for treating diseases.

2.10 Cell model

Sprague-Dawley (SD) rat BMSCs were generously supplied by the Stem Cell Bank, Chinese Academy of Sciences. These BMSCs were cultivated in growth medium consisting of α -MEM containing 10% FBS and antibiotics (HyClone, United States). Cultures were maintained at 37°C in a 5% CO₂ atmosphere. BMSCs assigned to the flight group were cultured in the Rotary Cell Culture System (RCCS, Synthecon Company, United States) for 72 h. During this period, the rotation speed was gradually increased from 10 to 20 ([Supplementary Figures 1, 2](#)).

4 <http://mirtarbase.mbc.nctu.edu.tw/php/index.php>

5 <https://string-db.org/>



2.11 Validation of key genes and ceRNA network by qRT-PCR

Total RNA was isolated using Easstep®-Super-Total-RNA-Extraction-Kit (Promega Biological Products, China). The yield of total RNA was examined using NanoDrop equipment (Thermo-Fisher-Scientific, United States). cDNA synthesis was performed using PrimeScript RT reagent Kit (Takara, Japan). Then, SYBR Green (TianGen, China) was employed to conduct qRT-PCR. All specific primer pairs (5' to 3') were shown as follows: (1) GAPDH: F: GGGTGTGAACCACGAGAAAT, R: ACTGTGGTCATGAGCCCTTC; (2) JPX: F: GCGAAGGTCTTGTCACATCTGTC, R: AGAGGAGGAAGGAAGGAAGGAAAC; (3) LINC01123: F: AGGAAGGAGGTGCTTGGCTCTC, R: TGAC AACGATGACGAGGAACTGAC; (4) LAMC1: F: TGGACTT ACTTGCTGACTCATTGACTG, R: ATTGATGGATGGATGGAT GGATGGATG; (5) LAMA4: F: AACTGACCGAGGCTGTCAAG, R: TGAGGTTTCTCACTGCGTCC. The relative expression of genes was determined using the $2^{-\Delta\Delta Ct}$ approach, with GAPDH serving as the internal control.

2.12 Statistical analysis

The findings obtained from qRT-PCR were analyzed by Student's *t*-test using GraphPad Prism 9.0 (GraphPad Software, Inc., United States). Statistical significance was deemed at a threshold of $P < 0.05$.

3 Results

3.1 Comparative analysis of miRNA and mRNA expression profiles in BMSCs from ground and flight samples

In this study, 1,027 significant DEmRNAs (622 with upregulation and 405 with downregulation) were identified using a significance threshold of $p < 0.05$ and a log₂-fold change of > 1 (Figures 2A–C). Additionally, 20 DEmiRNAs were discerned in BMSCs using the same criteria, comprising nine with downregulation and 11 with upregulation (Figures 2D–F). In total, 8,623 target mRNAs of the DEmiRNAs were estimated through miRecords, miRTarBase, and DIANA TarBase v.8.

3.2 Construction of co-expressed gene module for lncRNA-mRNA pairs

According to the expression's variance, the top 5,000 genes were first identified from flight samples in the GSE100930 dataset. Subsequently, through optimization, a soft threshold of $\beta = 12$ was determined, achieving an R^2 of 0.85 (Figures 3A, B). When the TOMType parameter in the WGCNA package was set to "signed," 21 modules were delineated via average linkage hierarchical clustering (Figures 3C, D). Ultimately, the analysis yielded 19,935

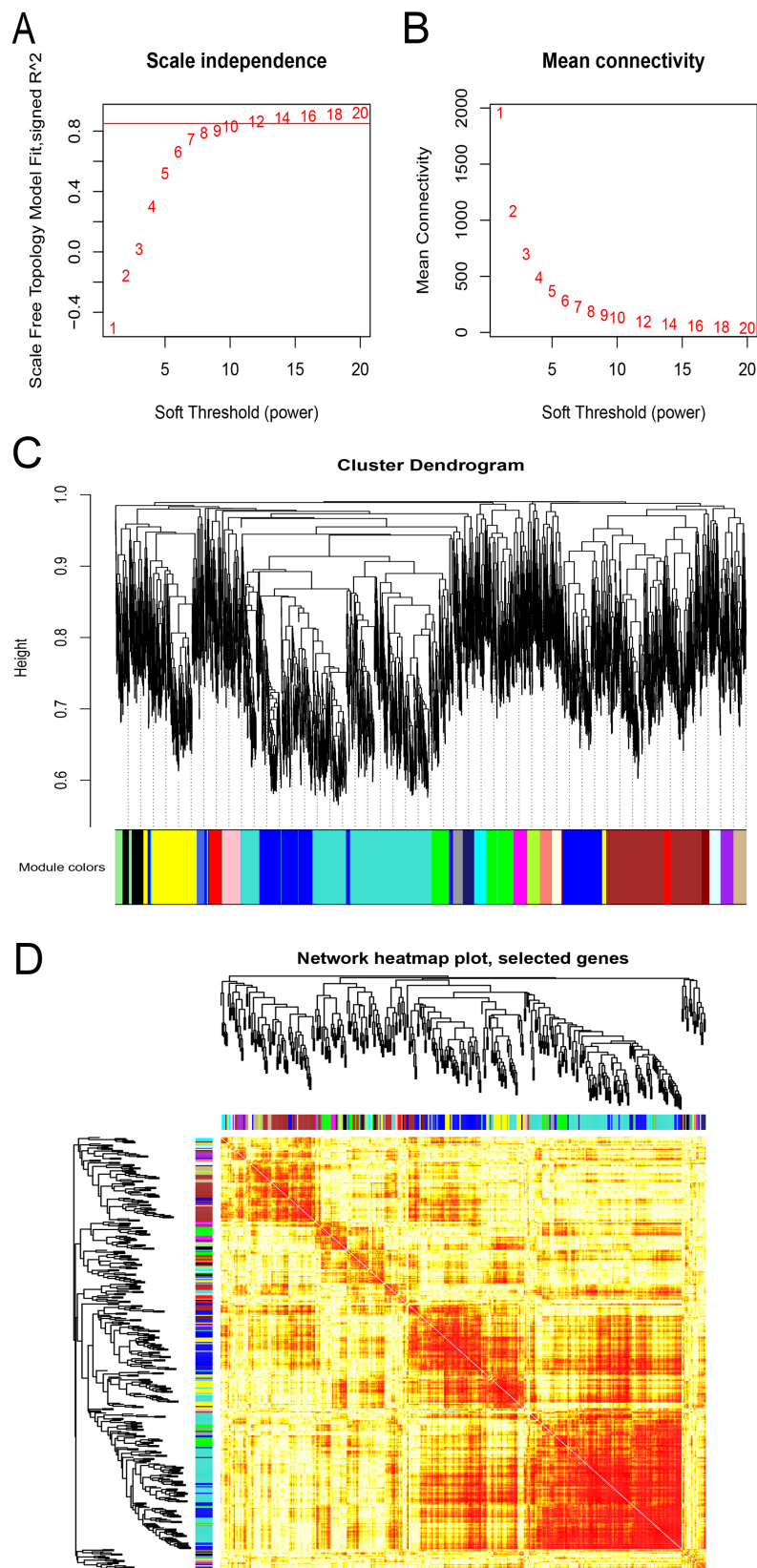
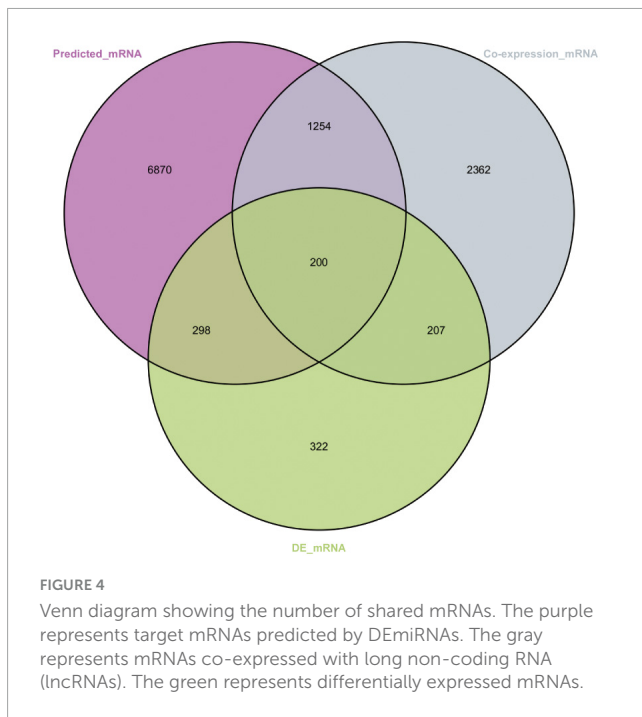


FIGURE 3

Weighted gene co-expression network analysis (WGCNA) of flight samples (GSE100930). **(A)** Assessment of scale-free fit indices across soft-thresholding powers (β). **(B)** Evaluation of mean connectivity across soft-thresholding powers. **(C)** The hierarchical clustering dendrogram was constructed according to the gene dissTOM. Each color-coded row beneath the dendrogram represents a distinct module, with module width indicating the number of co-expressed genes. **(D)** Visualization of inter-gene interactions within co-expression modules. Various colors on the vertical and horizontal axes denote diverse modules, while yellow hues denote inter-module correlations. Significant variations in correlation patterns among modules were observed.



positive lncRNA-mRNA co-expression pairs across these 21 signed modules, involving 95 lncRNAs and 4,023 mRNAs.

3.3 Establishment of the lncRNA-miRNA-mRNA network

A total of 200 shared mRNAs were obtained from positive lncRNA-mRNA co-expression pairs, predictive miRNA-mRNA expression pairs, and DE mRNAs (Figure 4). A total of 74 lncRNAs, 19 miRNAs and 200 mRNAs were then integrated into a lncRNA-miRNA-mRNA network by shared mRNAs (Figure 5), which consisted of 293 nodes and 2,075 edges.

3.4 Enrichment analysis

The 200 differentially expressed mRNAs (DE mRNAs) implicated in the competing endogenous RNA (ceRNA) network underwent enrichment analysis. Utilizing GO terms for Molecular Functions (MF), Cellular Compartments (CC), and Biological Processes (BP), the primary functions of these DE mRNAs were examined. Notably, significant enrichment was observed for GO terms associated with the collagen-containing extracellular matrix, extracellular matrix structural constituent, and extracellular matrix organization (Figure 6A). Conversely, enrichment analysis of downregulated genes highlighted terms associated with the endoplasmic reticulum chaperone complex and response to endoplasmic reticulum stress as the most significantly enriched (Figure 6B). These processes are likely involved in BMSC differentiation.

Moreover, KEGG pathways were employed for systematic gene characteristic analysis by integrating higher-level pathway information with gene data. Focal adhesion emerged as the most

highly enriched pathway among DE mRNAs with upregulation, whereas protein processing in the endoplasmic reticulum ranked as the most enriched pathway among DE mRNAs with downregulation (Figure 6C).

3.5 Establishment of PPI network and identification of hub genes

The selection of 10 hub genes was guided by the Cytohubba plug-in in Cytoscape. The genes, including nine upregulated genes and one downregulated gene, were then ranked according to their Maximal clique centrality (MCC) values (Figure 7). The key genes Laminin-Subunit-Gamma-1 (LAMC1) and Laminin-Subunit-Alpha-4 (LAMA4) were identified. Furthermore, from the constructed ceRNA network, three distinct mRNA-miRNA-lncRNA regulatory axes were delineated: LINC01123/hsa-let-7i-5p/LAMC1, JPX/hsa-miRNA-3619-5p/LAMA4, and LINC01123/hsa-miRNA-3619-5p/LAMA4. Detailed information regarding the two key lncRNAs, LINC01123 and JPX, is provided in Table 2.

3.6 CMap analysis

After submitting 200 DE mRNAs into the CMap Query, including 117 upregulated signatures and 83 downregulated signatures, three bioactive compounds (SB-216763, oxymetholone, flubendazole) were identified as candidate therapeutics for treating DOP since they had the lowest connectivity scores (Table 3).

3.7 Validation of key genes and ceRNA network in DOP

To validate the findings from the microarray analysis, qRT-PCR was employed to detect the expression levels of key genes and the ceRNA network (Figure 8). The microarray analysis indicated upregulation of LAMC1 and LAMA4 in the DOP condition. According to the competitive mechanism, their corresponding lncRNAs were expected to exhibit upregulation in DOP as well. The qRT-PCR results demonstrated high expression levels of JPX, LINC01123, LAMC1, and LAMA4 in the flight group, aligning with our anticipated outcomes.

4 Discussion

Disuse osteoporosis is a prevalent condition experienced by both astronauts during spaceflight and individuals with spinal cord injuries, contributing significantly to deleterious effects on human health (5, 17). It is widely recognized that a majority of human RNA transcripts do not encode proteins but rather play crucial roles in regulating cellular physiology and influencing cellular function. Recent advances in network biology have highlighted the importance of certain properties of biological networks (18), such as scale-free distribution and hierarchical modularization, in

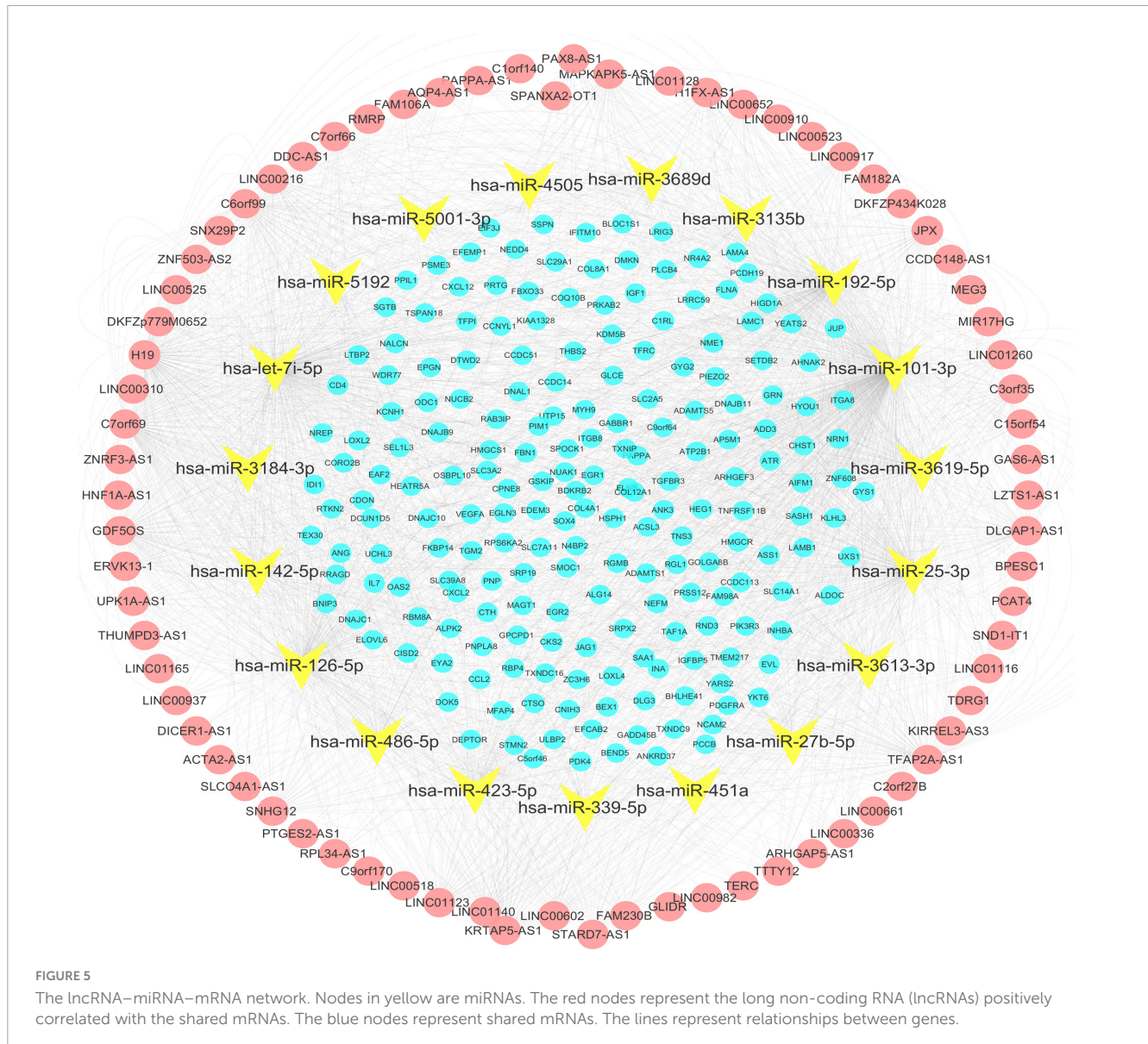


FIGURE 5
The lncRNA–miRNA–mRNA network. Nodes in yellow are miRNAs. The red nodes represent the long non-coding RNA (lncRNAs) positively correlated with the shared mRNAs. The blue nodes represent shared mRNAs. The lines represent relationships between genes.

maintaining the stability of cellular processes. This underscores the potential of regulatory network analysis to offer novel insights into the mechanisms underlying gene regulation and dysfunction in DOP. In this study, we present, for the first time, the construction of a ceRNA network for BMSCs in DOP, linking the functions of protein-coding mRNAs with non-coding RNAs, including lncRNAs and miRNAs.

Through functional enrichment analysis, we propose a hypothesis that following the cessation of mechanical stress, dysregulated lncRNAs may disrupt signaling pathways involved in endoplasmic reticulum (ER) stress and extracellular matrix (ECM) collagen production. This disruption, in turn, could impact bone mineral deposition, turnover, and osteocyte activity (19). ER stress, associated with cellular damage to the protein-folding mechanism, has been reported to inhibit osteoblast formation, increase osteoclast numbers, and enhance their migration and adhesion, consistent with our enrichment analysis findings (20). Notably, focal adhesion emerged as a significant term in both GO and KEGG analyses. Focal adhesion plays a crucial role in

mediating cellular interactions with the ECM and transducing mechanical forces and regulatory signals (21). Furthermore, *in vivo* studies have demonstrated the assembly of focal adhesion complexes in response to mechanical overload, suggesting its potential involvement in DOP development (22, 23). However, further investigation is warranted to validate this observation. This underscores the importance of understanding the effects of microgravity on osteoblast cytoskeletal adhesion and organization as well as osteoclast bone resorption in regulating DOP progression.

The PPI network analysis revealed two hub genes, LAMC1 and LAMA4. LAMC1, a pivotal member of the laminin family, interacts with integrins, promoting cell migration and adhesion (24). Additionally, LAMC1 plays a significant role in aging BMSCs (25). LAMA4, a key component of the bone marrow ECM, influences the proliferation and survival of stem and progenitor cells (26). Both hub genes are associated with the ECM term (GO: 0031012) in GO analysis. The mineralization process of bone tissue exhibits unique biomechanical properties, and the investigation into vertebrate extracellular matrix mineralization remains a focal

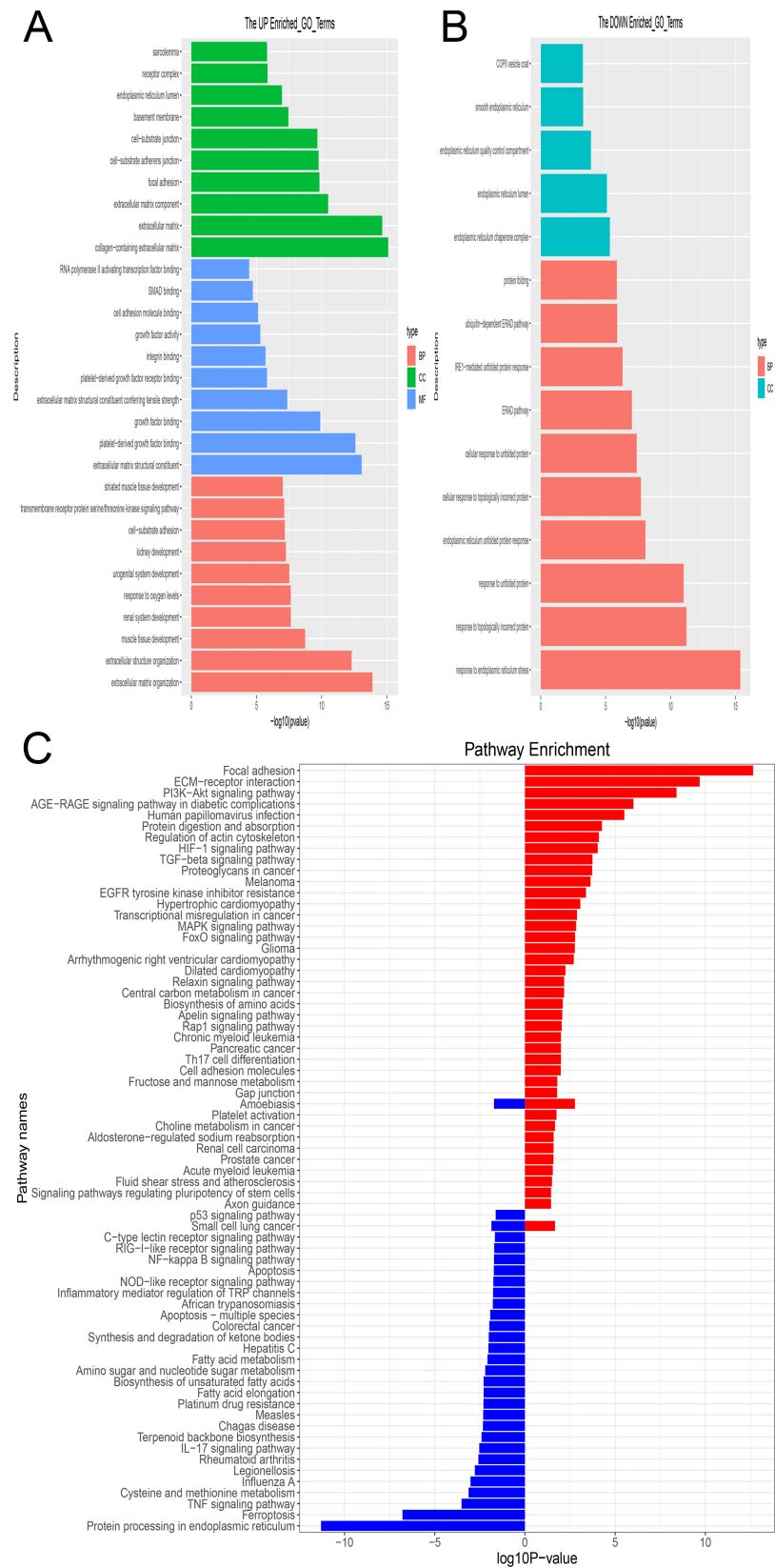


FIGURE 6

The enrichment analysis of shared mRNA. (A,B) GO enrichment analysis was performed across three functional categories: Molecular Functions (MF), Cellular Compartments (CC) and Biological Processes (BP). Panel (A) indicates enrichment by upregulated genes, while Panel (B) indicates enrichment by downregulated genes. The y-axis denotes the enriched GO term, while the x-axis denotes the corresponding p-value.

(C) Enrichment analysis of shared mRNAs using the KEGG pathways. The enriched pathway is depicted in red, comprising upregulated genes, while the enriched pathway is shown in blue, comprising downregulated genes.

TABLE 2 Basic information on the two long non-coding RNAs (lncRNAs).

LncRNA	Entrez_ID	Locus	Genomic length	Strand
JPX	554203	chrX:73,944,182-74,070,832	126651	+
LINC01123	440894	chr2:109,986,583-109,996,414	9832	+

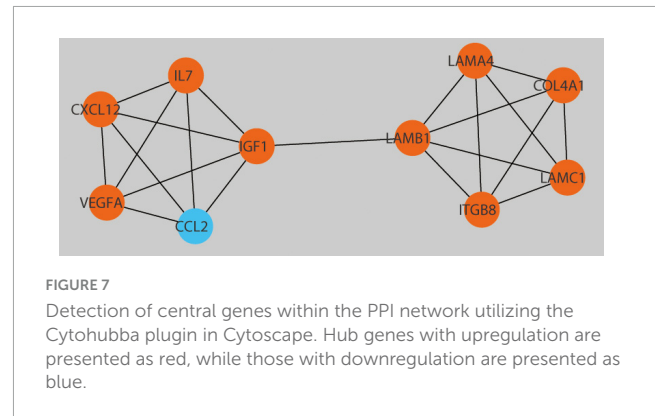
point in research (27). Bone comprises hundreds of ECM proteins, and the ECM of various bone tissue compartments directs bone remodeling through the coordinated actions of osteoblasts and osteoclasts (28). Exploring key genes within the ECM could elucidate its role in DOP.

In our study, two key regulatory axes, JPX/hsa-miR-3619-5p/LAMA4 and LINC01123/hsa-let-7i-5p/LAMC1, were identified as critical modulators of ECM remodeling and bone homeostasis. Both JPX and LINC01123 function as competitive endogenous RNAs (ceRNAs), sequestering miRNAs to prevent the suppression of LAMA4 and LAMC1, two essential ECM components. This enhances ECM structural stability, promotes osteoblast attachment and proliferation, and modulates osteoclast activity, thereby influencing bone metabolism.

The lncRNA JPX, known as an activator of Xist, can activate Xist both in trans and cis (29). XIST has been implicated in promoting osteoporosis by inhibiting the differentiation of BMSCs (30, 31). Moreover, the Wnt/ β -catenin pathway, crucial for DOP development, may be activated by hsa-miR-3619-5p through enhancing the stability of β -catenin (32). Our findings suggest that JPX, acting as a ceRNA, modulates hsa-miR-3619-5p levels, influencing the expression of LAMA4 and the remodeling of ECM. Dysregulation of this axis could destabilize bone matrix integrity and disrupt osteoblast and osteoclast activity. Activation of Wnt signaling via hsa-miR-3619-5p may partially mitigate bone loss associated with DOP, presenting a potential therapeutic strategy. The JPX/hsa-miR-3619-5p/LAMA4 axis thus emerges as a critical regulatory mechanism in ECM remodeling and DOP progression.

Previous studies have demonstrated the ceRNA crosstalk network involving LINC01123, which acts as a decoy to sequester miRNA-199a-5p from binding c-Myc mRNA, thereby attenuating its suppressive effect on c-Myc expression (33). Although hsa-let-7i-5p has not been extensively studied in bone-related research, it has shown potential as a diagnostic and predictive biomarker in other disease models (34, 35). Further investigation is warranted to elucidate the potential functions of these lncRNAs and miRNAs. In our study, LINC01123 was identified as a competitive endogenous RNA (ceRNA) that sequesters hsa-let-7i-5p, thereby upregulating LAMC1 expression and supporting ECM integrity. Dysregulation of this axis, particularly the overexpression of LINC01123, could impair osteoblast differentiation and enhance osteoclast activity, disrupting bone matrix mineralization and turnover. This dysregulation may exacerbate the pathological progression of disuse osteoporosis (DOP), highlighting the critical role of the LINC01123/hsa-let-7i-5p/LAMC1 axis in maintaining bone homeostasis under mechanical unloading conditions.

Based on CMap analysis, three chemicals, namely, SB-216763, Oxymetholone, and Flubendazole, emerged as potential therapeutic



agent for treating DOP. SB-216763, an inhibitor of glycogen synthase kinase 3 (GSK-3), regulates osteoclast differentiation by phosphorylating NFATc1. Moreover, GSK-3, activated by dexamethasone, inhibits the osteoblast differentiation-related cell cycle (36–38). Notably, GSK-3 also plays a crucial role in the Wnt/ β -catenin axis, a potential target for osteoporosis treatment (39, 40). Therefore, SB-216763 holds promise as a significant drug candidate for DOP treatment.

Oxymetholone is an androgen and anabolic steroid (AAS) which is used for treating osteoporosis (41). Its anabolic effects are mediated through androgen receptor activation, which stimulates protein synthesis and mineral deposition in bone tissue. Oxymetholone has a well-established clinical history in treating osteoporosis and other conditions associated with bone fragility. Its ability to enhance bone mass and strength makes it a valuable option for managing severe DOP, particularly in patients with significant bone loss due to prolonged immobilization. Our data were consistent with previous results; and to avoid repetition of previously published discussion, the data will not be examined in depth here.

Flubendazole, a tubulin inhibitor, has been extensively evaluated in humans and animals for the treatment of intestinal parasites and systemic worm infections. Tubulin is a major component of microtubules, which are cytoskeletal components needed for cell division, cell transport, and cell integrity (42). The microtubule-disrupting mechanism underpinning flubendazole's antiproliferative effects has garnered significant interest in oncology research. Preclinical studies have demonstrated its broad-spectrum anti-tumor efficacy across diverse malignancies (43, 44). In addition, previous studies showed that another tubulin inhibitor vinpocetine had a similar binding domain like that for flubendazole, and was shown to inhibit RANKL-induced osteoclastogenesis and thereby attenuate bone loss (45). However, the direct effects of flubendazole on bone metabolism, particularly concerning osteoblasts and osteoclasts, remain inadequately explored. As a benzimidazole anthelmintic agent, flubendazole demonstrates a well-established safety profile at standard therapeutic doses, with minimal incidence of severe adverse reactions in clinical practice (46, 47). However, its pharmacological safety requires rigorous reassessment when considering potential applications in bone disorders, particularly in the context of bone-related pathologies where drug-bone cell interactions remain undefined. That flubendazole may be a

TABLE 3 Three compounds with high negative connectivity scores in Connectivity Map (CMap) analysis.

Name	ID	Target	Score	MOA
SB-216763	BRD-K59184148	GSK3B, CCNA2, CDK2, GSK3A	-97.86	Glycogen synthase kinase inhibitor
Oxymetholone	BRD-A23637604	AR	-97.55	Androgen receptor agonist
Flubendazole	BRD-K86003836	TUBB	-96.54	Tubulin inhibitor

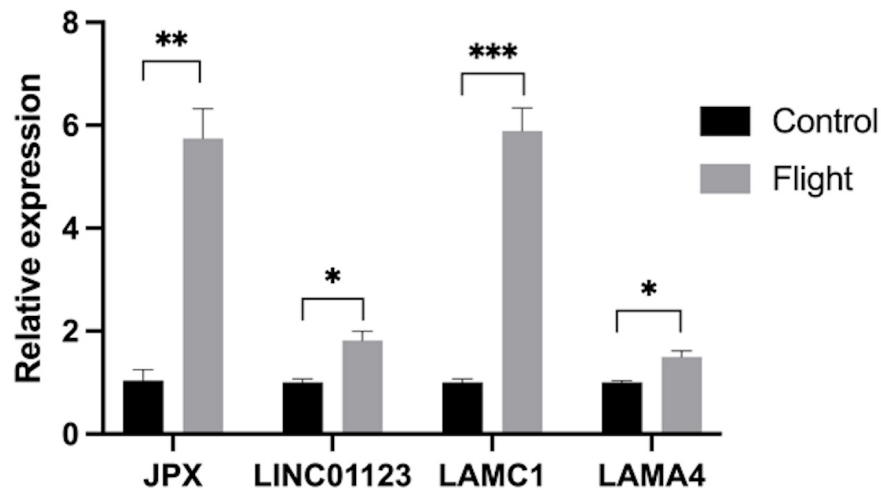


FIGURE 8

Expression of JPX, LINC01123, LAMC1 and LAMA4 in samples from rats in the flight group (in gray) and the control group (in black) (* $P < 0.05$, ** $P < 0.01$, *** $P < 0.001$).

potential drug for reducing bone loss after DOP is also worthy of further study.

However, we acknowledge several limitations in this research. Firstly, the sample size of BMSCs in the dataset was small, although it met the statistical significance requirements for biological duplication. The relatively small sample size may limit the robustness of miRNA differential expression analysis and we will integrate larger datasets in future research to enhance the reliability of the results. Secondly, although we constructed the ceRNA network, further investigation is needed to elucidate the precise mechanisms of action of these lncRNAs, miRNAs, and mRNAs through targeted studies. Integrating more data in the future will enhance the accuracy and completeness of the ceRNA network. As our future direction, we aim to explore the direct molecular biological mechanisms of DOP-specific ceRNAs and how dysregulated ECM remodeling contributes to DOP. Additionally, further studies on bioactive compounds will investigate their potential in translational medicine.

5 Conclusion

In conclusion, through bioinformatics analysis of BMSC gene expression data under microgravity conditions, we constructed the first mRNA-miRNA-lncRNA network. This network sheds light on the potential role of ceRNA in regulating BMSCs under microgravity and provides novel insights into the regulatory mechanisms and therapeutic targets for DOP.

Data availability statement

The original contributions presented in this study are included in this article/Supplementary material, further inquiries can be directed to the corresponding author.

Ethics statement

Ethical approval was not required for the studies on humans in accordance with the local legislation and institutional requirements because only commercially available established cell lines were used.

Author contributions

WW: Validation, Writing – original draft, Writing – review and editing. ZZ: Funding acquisition, Writing – original draft. BL: Data curation, Writing – original draft, Writing – review and editing. ZF: Validation, Visualization, Writing – original draft. JL: Funding acquisition, Writing – review and editing.

Funding

The author(s) declare that financial support was received for the research and/or publication of this article. This work was supported by National Key Research and Development Program of

China (2023YFC2507605), Foundation of Tianjin Science Technology Key Project (21JCZDJC01000), and The Key Laboratory of Basic Research on Prevention and Treatment of Birth Defects in Guangxi (GXWCH-ZDKF-2022-22).

Acknowledgments

We authors would like to express their gratitude to EditSprings (<https://www.editsprings.com/>) for the expert linguistic services provided.

Conflict of interest

The authors declare that the research was conducted in the absence of any commercial or financial relationships that could be construed as a potential conflict of interest.

References

- Grimm D, Grosse J, Wehland M, Mann V, Reseland J, Sundaresan A, et al. The impact of microgravity on bone in humans. *Bone*. (2016) 87:44–56. doi: 10.1016/j.bone.2015.12.057
- Klein-Nulend J, Bacabac R, Veldhuijzen J, Van Loon J. Microgravity and bone cell mechanosensitivity. *Adv Space Res*. (2003) 32:1551–9. doi: 10.1016/S0273-1177(03)90395-4
- Baek K, Barlow A, Allen M, Bloomfield S. Food restriction and simulated microgravity: Effects on bone and serum leptin. *J Appl Physiol*. (1985) 104:1086–93. doi: 10.1152/jappphysiol.01209.2007
- Vernikos J, Schneider V. Space, gravity and the physiology of aging: Parallel or convergent disciplines? A mini-review. *Gerontology*. (2010) 56:157–66. doi: 10.1159/000252852
- Alexandre C, Vico L. Pathophysiology of bone loss in disuse osteoporosis. *Joint Bone Spine*. (2011) 78:572–6. doi: 10.1016/j.jbspin.2011.04.007
- Pittenger M, Mackay A, Beck S, Jaiswal R, Douglas R, Mosca J, et al. Multilineage potential of adult human mesenchymal stem cells. *Science*. (1999) 284:143–7. doi: 10.1126/science.284.5411.143
- Ding D, Shyu W, Lin S. Mesenchymal stem cells. *Cell Transplant*. (2011) 20:5–14. doi: 10.3727/096368910X
- Mabuchi Y, Houlihan D, Akazawa C, Okano H, Matsuzaki Y. Prospective isolation of murine and human bone marrow mesenchymal stem cells based on surface markers. *Stem Cells Int*. (2013) 2013:507301. doi: 10.1155/2013/507301
- Chen Q, Shou P, Zheng C, Jiang M, Cao G, Yang Q, et al. Fate decision of mesenchymal stem cells: Adipocytes or osteoblasts? *Cell Death Differ*. (2016) 23:1128–39. doi: 10.1038/cdd.2015.168
- Mercer T, Dinger M, Mattick J. Long non-coding RNAs: Insights into functions. *Nat Rev Genet*. (2009) 10:155–9. doi: 10.1038/nrg2521
- Sun L, Goff L, Trapnell C, Alexander R, Lo K, Hacisuleyman E, et al. Long noncoding RNAs regulate adipogenesis. *Proc Natl Acad Sci U S A*. (2013) 110:3387–92. doi: 10.1073/pnas.1222643110
- Yuan Y, Zhang L, Tong X, Zhang M, Zhao Y, Guo J, et al. Mechanical stress regulates bone metabolism through MicroRNAs. *J Cell Physiol*. (2017) 232:1239–45. doi: 10.1002/jcp.25688
- Salmena L, Poliseno L, Tay Y, Kats L, Pandolfi PP. A ceRNA hypothesis: The Rosetta Stone of a hidden RNA language? *Cell*. (2011) 146:353–8. doi: 10.1016/j.cell.2011.07.014
- Ringnér M. What is principal component analysis? *Nat Biotechnol*. (2008) 26:303–4. doi: 10.1038/nbt0308-303
- Ficklin S, Luo F, Feltus F. The association of multiple interacting genes with specific phenotypes in rice using gene coexpression networks. *Plant Physiol*. (2010) 154:13–24. doi: 10.1104/pp.110.159459
- Lamb J, Crawford ED, Peck D, Modell J, Blat I, Wrobel M, et al. The connectivity map: Using gene-expression signatures to connect small molecules, genes, and disease. *Science*. (2006) 313:1929–35. doi: 10.1126/science.1132939
- Hughes-Fulford M. To infinity and beyond! Human spaceflight and life science. *FASEB J*. (2011) 25:2858–64. doi: 10.1096/fj.11-0902ufm
- Panni S, Lovering R, Porras P, Orchard S. Non-coding RNA regulatory networks. *Biochim Biophys Acta Gene Regul Mech*. (2020) 1863:194417. doi: 10.1016/j.bbagr.2019.194417
- Walter P, Ron D. The unfolded protein response: From stress pathway to homeostatic regulation. *Science*. (2011) 334:1081–6. doi: 10.1126/science.1209038
- Li J, Yang S, Li X, Liu D, Wang Z, Guo J, et al. Role of endoplasmic reticulum stress in disuse osteoporosis. *Bone*. (2017) 97:2–14. doi: 10.1016/j.bone.2016.12.009
- Chen C, Alonso J, Ostuni E, Whitesides G, Ingber D. Cell shape provides global control of focal adhesion assembly. *Biochem Biophys Res Commun*. (2003) 307:355–61. doi: 10.1016/S0006-291X(03)01165-3
- Torsoni A, Fonseca P, Crosara-Alberto D, Franchini K. Early activation of p160ROCK by pressure overload in rat heart. *Am J Physiol Cell Physiol*. (2003) 284:C1411–9. doi: 10.1152/ajpcell.00098.2002
- Franchini K, Torsoni A, Soares P, Saad M. Early activation of the multicomponent signaling complex associated with focal adhesion kinase induced by pressure overload in the rat heart. *Circ Res*. (2000) 87:558–65. doi: 10.1161/01.res.87.7.558
- Kawataki T, Yamane T, Naganuma H, Rousselle P, Andurén I, Tryggvason K, et al. Laminin isoforms and their integrin receptors in glioma cell migration and invasiveness: Evidence for a role of alpha5-laminin(s) and alpha3beta1 integrin. *Exp Cell Res*. (2007) 313:3819–31. doi: 10.1016/j.yexcr.2007.07.038
- Yoo J, Kim C, Jung H, Lee D, Kim J. Discovery and characterization of miRNA during cellular senescence in bone marrow-derived human mesenchymal stem cells. *Exp Gerontol*. (2014) 58:139–45. doi: 10.1016/j.exger.2014.07.020
- Susek K, Korpos E, Huppert J, Wu C, Savelyeva I, Rosenbauer F, et al. Bone marrow laminins influence hematopoietic stem and progenitor cell cycling and homing to the bone marrow. *Matrix Biol*. (2018) 67:47–62. doi: 10.1016/j.matbio.2018.01.007
- Murshed M. Mechanism of bone mineralization. *Cold Spring Harb Perspect Med*. (2018) 8:a031229. doi: 10.1101/cshperspect.a031229
- Alford A, Kozloff K, Hankenson K. Extracellular matrix networks in bone remodeling. *Int J Biochem Cell Biol*. (2015) 65:20–31. doi: 10.1016/j.biocel.2015.05.008
- Carmona S, Lin B, Chou T, Arroyo K, Sun S. lncRNA Jpx induces Xist expression in mice using both trans and cis mechanisms. *PLoS Genet*. (2018) 14:e1007378. doi: 10.1371/journal.pgen.1007378
- Chen X, Yang L, Ge D, Wang W, Yin Z, Yan J, et al. Long non-coding RNA XIST promotes osteoporosis through inhibiting bone marrow mesenchymal stem cell differentiation. *Exp Ther Med*. (2019) 17:803–11. doi: 10.3892/etm.2018.7033
- Niu S, Xiang F, Jia H. Downregulation of lncRNA XIST promotes proliferation and differentiation, limits apoptosis of osteoblasts through regulating miR-203-3p/ZFPM2 axis. *Connect Tissue Res*. (2021) 62:381–92. doi: 10.1080/03008207.2020.1752200
- Yu S, Cao S, Hong S, Lin X, Guan H, Chen S, et al. miR-3619-3p promotes papillary thyroid carcinoma progression via Wnt/ β -catenin pathway. *Ann Transl Med*. (2019) 7:643. doi: 10.21037/atm.2019.10.71

Publisher's note

All claims expressed in this article are solely those of the authors and do not necessarily represent those of their affiliated organizations, or those of the publisher, the editors and the reviewers. Any product that may be evaluated in this article, or claim that may be made by its manufacturer, is not guaranteed or endorsed by the publisher.

Supplementary material

The Supplementary Material for this article can be found online at: <https://www.frontiersin.org/articles/10.3389/fmed.2025.1444165/full#supplementary-material>

33. Hua Q, Jin M, Mi B, Xu F, Li T, Zhao L, et al. LINC01123, a c-Myc-activated long non-coding RNA, promotes proliferation and aerobic glycolysis of non-small cell lung cancer through miR-199a-5p/c-Myc axis. *J Hematol Oncol.* (2019) 12:91. doi: 10.1186/s13045-019-0773-y
34. Huang R, Meng T, Chen R, Yan P, Zhang J, Hu P, et al. The construction and analysis of tumor-infiltrating immune cell and ceRNA networks in recurrent soft tissue sarcoma. *Aging (Albany NY).* (2019) 11:10116–43. doi: 10.18632/aging.102424
35. Zhang K, Yang R, Chen J, Qi E, Zhou S, Wang Y, et al. Let-7i-5p regulation of cell morphology and migration through distinct signaling pathways in normal and pathogenic urethral fibroblasts. *Front Bioeng Biotechnol.* (2020) 8:428. doi: 10.3389/fbioe.2020.00428
36. Kim H, He L, Lee S, Park C, Kim D, Han H, et al. Inhibition of osteoclasts differentiation by CDC2-induced NFATc1 phosphorylation. *Bone.* (2020) 131:115153. doi: 10.1016/j.bone.2019.115153
37. Smith E, Frenkel B. Glucocorticoids inhibit the transcriptional activity of LEF/TCF in differentiating osteoblasts in a glycogen synthase kinase-3beta-dependent and -independent manner. *J Biol Chem.* (2005) 280:2388–94. doi: 10.1074/jbc.M406294200
38. Yun S, Yoon H, Jeong S, Chung Y. Glucocorticoid induces apoptosis of osteoblast cells through the activation of glycogen synthase kinase 3beta. *J Bone Miner Metab.* (2009) 27:140–8. doi: 10.1007/s00774-008-0019-5
39. Liu H, Guo Y, Zhu R, Wang L, Chen B, Tian Y, et al. Fructus ligustri lucidi preserves bone quality through induction of canonical Wnt/ β -catenin signaling pathway in ovariectomized rats. *Phytother Res.* (2021) 35:424–41. doi: 10.1002/ptr.6817
40. Wang Y, Chen J, Chen J, Dong C, Yan X, Zhu Z, et al. Daphnetin ameliorates glucocorticoid-induced osteoporosis via activation of Wnt/GSK-3 β / β -catenin signaling. *Toxicol Appl Pharmacol.* (2020) 409:115333. doi: 10.1016/j.taap.2020.115333
41. Vose G, Keele D, Milner A, Rawley R, Roach T, Sprinkle E. Effect of sodium fluoride, inorganic phosphate, and oxymetholone therapies in osteoporosis: A six-year progress report. *J Gerontol.* (1978) 33:204–12. doi: 10.1093/geronj/33.2.204
42. Jordan M, Wilson L. Microtubules as a target for anticancer drugs. *Nat Rev Cancer.* (2004) 4:253–65. doi: 10.1038/nrc1317
43. Zhen Y, Zhao R, Wang M, Jiang X, Gao F, Fu L, et al. Flubendazole elicits anti-cancer effects via targeting EVA1A-modulated autophagy and apoptosis in Triple-negative breast cancer. *Theranostics.* (2020) 10:8080–97. doi: 10.7150/thno.43473
44. Zhou X, Zou L, Chen W, Yang T, Luo J, Wu K, et al. Flubendazole, FDA-approved anthelmintic, elicits valid antitumor effects by targeting P53 and promoting ferroptosis in castration-resistant prostate cancer. *Pharmacol Res.* (2021) 164:105305. doi: 10.1016/j.phrs.2020.105305
45. Zhu M, Liu H, Sun K, Liu J, Mou Y, Qi D, et al. Vinpocetine inhibits RANKL-induced osteoclastogenesis and attenuates ovariectomy-induced bone loss. *Biomed Pharmacother.* (2020) 123:109769. doi: 10.1016/j.biopha.2019.109769
46. Téllez-Girón E, Ramos M, Dufour L, Montante M, Tellez E, Rodríguez J, et al. Treatment of neurocysticercosis with flubendazole. *Am J Trop Med Hyg.* (1984) 33:627–31. doi: 10.4269/ajtmh.1984.33.627
47. Feldmeier H, Bienzle U, Döhning E, Dietrich M. Flubendazole versus mebendazole in intestinal helminthic infections. *Acta Trop.* (1982) 39:185–9.